Flow Structure of the Wake behind an Elliptic Cylinder Close to a Free Surface

Daichin, Sang Joon Lee*

Department of Mechanical Engineering, Pohang University of Science and Technology (POSTECH)
Kyungbuk, Pohang 790-784, Korea

The flow fields around an elliptic cylinder of axis ratio AR=2 adjacent to a free surface were investigated experimentally using a water channel. The main objective is to understand the effect of the free surface on the flow structure in the near-wake. The flow fields were measured by varying the depth of cylinder submergence, for each experimental condition, 350 velocity fields were measured using a single-frame PIV system and ensemble-averaged to obtain the spatial distribution of turbulent statistics. For small submergence depths a large-scale eddy structure was observed in the near-wake, causing a reverse flow near the free surface, downstream of the cylinder. As the depth of cylinder submergence was increased, the flow speed in the gap region between the upper surface of the cylinder and the free surface increased and formed a substantial jet flow. The general flow structure of the elliptic cylinder is similar to previous results for a circular cylinder submerged near to a free surface. However, the width of the wake and the angle of downward deflection of the shear layer developed from the lower surface of the elliptic cylinder are smaller than those for a circular cylinder.

Key Words : Elliptic Cylinder, PIV, Flow Field, Free Surface, Near Wake

1. Introduction

The flow structure of the wake behind a circular cylinder has been extensively studied due to the simple geometry and wide practical applications of these cylinders, and because of academic interest in flow characteristics such as vortex shedding. Recently, the flow interaction between the turbulent boundary layer over a flat plate and the wake behind a cylinder located nearby has become a research topic of interest. Bearman & Zdravkovich (1978) measured the pressure distribution and vortex shedding of a circular cylinder embedded in a boundary layer over a flat plate for a range of gap ratios. Vortex

shedding was found to be restricted for gaps smaller than a critical gap ratio of 0.3, and the Strouhal number (St) was almost constant for gap ratios greater than the critical gap ratio. Angrilli & Bergamaschi (1982) investigated the gap effect on vortex shedding from a circular cylinder and found that the vortex shedding frequency increases with decreasing gap ratio.

The effect of a free surface on the flow around an adjacent circular cylinder has recently been studied numerically and experimentally. Lin et al. (1996) studied the flow field of a vertical oscillating cylinder penetrates through a free water surface, the resulting flow field revealed that several patterns of nearly symmetrical vortices occurred during an oscillation cycle. Lin et al. (1995) also experimentally investigated the effect of Reynolds number (from 10^3 to 10^4) on the instantaneous structure of the near-wake of a circular cylinder using the PIV technique, and related this effect to the time-averaged representations of the loading on the cylinder.

---
* Corresponding Author,
  E-mail : sjlee@postech.ac.kr
  TEL : +82-54-279-2169; FAX : +82-54-279-3199
  Department of Mechanical Engineering, Pohang University of Science and Technology (POSTECH) Kyungbuk, Pohang, 790-784, Korea. (Manuscript Re -eived August 13, 2001; **Revised** September 30, 2001)

Sheridan et al. (1996) found that vortices generated from the free surface close to a cylinder formed a jet-like flow. The instantaneous vortices shed either side of the jet were found to be rapidly balanced after the onset of separation from the free surface.

The elliptic cylinder has a geometric shape and flow characteristics between those of a circular cylinder and a flat plate. Chio & Lee (2000) carried out a series of experiments to investigate the ground effect on the flow around elliptic cylinders in a turbulent boundary layer over a flat plane for various gap distances between the cylinders and ground. It was found that as the gap ratio increases the drag coefficient of the cylinder increases, but the lift coefficient decreases over the range of gap ratios tested. The drag coefficient of an elliptic cylinder is about half that of the corresponding circular cylinder. At small gap ratios the flow passing through the gap is constrained and the wake region behind the elliptic cylinder is smaller than that behind the circular cylinder.

However, no previous study has investigated the interaction between a free surface and an elliptic cylinder near to this surface. The main objective of the present study was to elucidate the flow structure of the near wake of an elliptic cylinder located near a free water surface with varying submergence depth of the cylinder.

2. Experimental Apparatus and Methods

The experiments were carried out in a circulating water channel with a test-section of width 300mm, depth 250mm and length 1.5m.

An elliptic cylinder with an axis ratio (**AR**, the ratio of major axis to minor axis of the cylinder) of 2 was mounted horizontally beneath the free surface, as shown in Fig. 1. The major and minor axes of the elliptic cylinder were $A = 28.2$mm and $B = 14.1$mm, respectively. The span(W) of the elliptic cylinder was 300mm and the corresponding aspect ratio (W/B) is about 21.3. Since the aspect ratio is larger than the nominal value showing 2-D flow structure, the three-
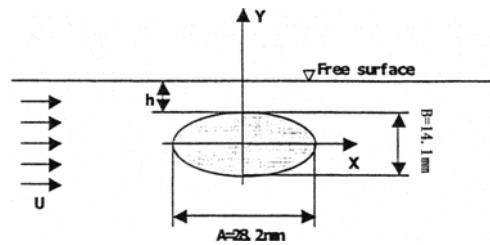

Fig. 1 Definition of flow and geometrical parameters

dimensional flow effect is nearly negligible in the center region of the wake. The gap between the upper surface of the cylinder and free water surface indicates the submergence depth (**h**), while the gap ratio is defined as $h^* = h/B$.

The instantaneous velocity vector fields were measured using a single-frame double-exposure PIV system; the experimental arrangement for the PIV measurements is illustrated as Fig. 2. The PIV system includes a high speed CCD camera that capture images with a resolution of 2048×2048 pixel^2 at 4 fps (frames per second), a dual-head Nd:YAG laser which gives a pulse energy of 25mJ, a synchronizer and optics. The Nd:YAG laser and high resolution CCD camera are synchronized using a control circuit. In the PIV velocity field measurements, two successive particle images can be recorded either on separate frames or on a single frame. The single-frame recording method using double exposures has the inherent problem of directional ambiguity in the determination of the velocity vectors. The CCD camera used in this study has a special built-in image-shifting feature that is ideal for resolving the directional ambiguity problem. During the first exposure of the CCD camera the particle image obtained by the first laser pulse is recorded on the CCD cell. During the time interval (t between consecutive laser pulses, the pixel lines of the CCD sensor array are translated a predetermined number of pixel lines. In the present work the record image was shifted 9 pixels. Details of the single-frame PIV velocity field measurement technique is described by Shin et al. (2000). Vestosint®1118 particles of diameter 37μm were seeded into the working fluid as
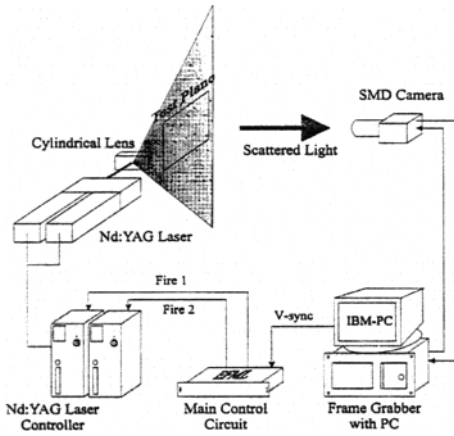
Fig. 2 Schematic diagram of the experimental arrangement

tracer particles. A thin laser light sheet was formed by passing the laser pulse through cylindrical and spherical lenses. The flow field around the cylinder model was illuminated from the bottom by the laser light sheet. Because of this geometry clear particle images could not be obtained from a part of the flow field above the cylinder.

In this study, the interrogation window size was 64×64 pixel^2 and the velocity vectors were calculated every 32 pixels, i. e. with 50% overlap between neighbor windows. The particle images in the two selected interrogation windows were then correlated, giving three correlation peaks with the largest peak at the center. Since the field of view is approximately 5 times the minor axis of the elliptic cylinder (B), the size of the interrogation area is 1.09mm × 1.09mm. Spatial distributions of turbulence statistics, including turbulence intensities, were obtained by ensemble averaging 350 instantaneous velocity fields. The turbulent kinetic energy was estimated as follow using the assumption of isotropic flow structure.

$$\frac{1}{2}q^2 = \frac{1}{2}(\overline{u'^2} + \overline{v'^2} + \overline{w'^2}) \approx \frac{3}{4}(\overline{u'^2} + \overline{v'^2})$$

Therefore, the real turbulent kinetic energy will be a little different from the present result at the regions where the isotropic assumption is not fulfilled.

The free stream was fixed at U=217mm/s,

Table 1 Experimental conditions

Gap h (mm)	0	2.0	6.0	10.0	13.0	16.0
Gap ratio $h^* = h/B$	0	0.142	0.425	0.709	0.92	1.13
Froude number $U/(gh)^{1/2}$	∞	1.55	0.89	0.69	0.61	0.55

which corresponds to a Reynolds number (UB/v) of about 2900. The gap ratio was varied in the range $0 \leq h/B \leq 1.13$, and the experimental conditions are shown in Table 1.

3. Results and Discussion

3.1 Instantaneous velocity fields

Instantaneous velocity fields of the flow around the elliptic cylinder were measured by varying the gap ratio h/B. For the larger gap ratios tested in this study (h^*=0.709, 0.92 and 1.13), the overall flow did not vary markedly, and the flow phenomena for the smaller gap ratios (h^*=0 and 0.142) were also similar to each other. We therefore concentrate our discussion on the flow structures for three gap ratios, h^*=0.142, 0.425 and 0.709, because these cases show completely different flow phenomena. The distortion of the free surface is ignored in the analysis of the results. To investigate the effect of the free surface on the near-wake of the elliptic cylinder, we first describe the flow characteristics of the instantaneous velocity fields for the three typical gap ratios.

Figures 3 and 4 show instantaneous velocity fields and streamline contours for three gap ratios of cylinder submergence, h^*=0.142, 0.425 and 0. 709. For the smallest submergence, h^*=0.142, the elliptic cylinder and free surface block the flow passing through the gap. As shown in Fig. 3(a), the flow from the bottom of the cylinder has a higher velocity than that at the top. This causes the formation of a mixing layer behind the cylinder, and entrains ambient fluid into the cylinder wake with going downstream. To maintain mass balance in the near-wake the flow beneath the free surface moves upstream and causes a reverse flow to compensate for the mass loss in the wake region, leading to the formation
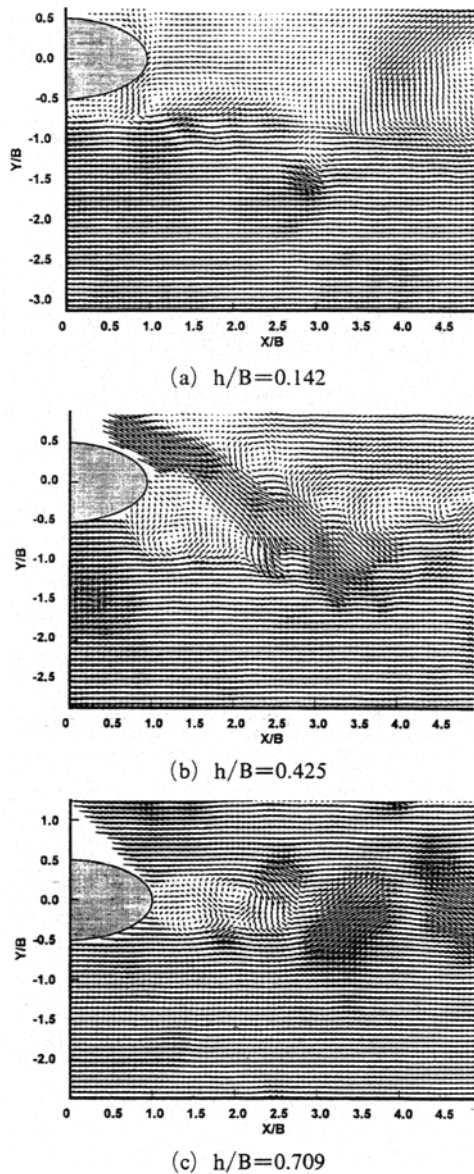
(a) h/B=0.142

(b) h/B=0.425

(c) h/B=0.709

Fig. 3 Instantaneous velocity fields with respect to the depth of submergence

of a large-scale swirl in the wake of the elliptic cylinder. The influence of this reverse flow deflects the mixing layer downward. While the restricted gap flow causes a Coanda effect at upper surface of the cylinder, it is weak and its velocity is lower than that at the bottom of the cylinder. When the cylinder submergence is increased to $h^*=0.425$ (Fig. 3(b)), the flow structure changes substantially from that at $h^*=$

0.142. The increased influx at the gap brings about a detachment of the flow from the upper surface of the cylinder and the formation of a substantial jet flow in this region. This jet flow is inclined downward and merges with the shear flow that develops from the bottom of the elliptic cylinder. The shear flow is enhanced by the substantial jet flow and forms counter-rotating vortices at both sides of the jet flow. However, the jet velocity is still lower than the velocity just below the cylinder. The entrainment of ambient fluid into the cylinder wake is intensified by mixing with the jet flow, causing a reverse flow in the proximity of the free surface and the formation of a large counter-clockwise vortex in the region close to the elliptic cylinder. The angle of downward deflection of the wake is slightly lower than at $h^*=0.142$.

On further increase of the depth of submergence to $h^*=0.709$ (Fig. 3(c)), the flow structure becomes similar to flow around a fully immersed blunt body. Vortices are shed alternately from the upper and lower sides of the cylinder and form a kind of Karman vortex street. However, the difference in flow velocity near the top and bottom of the cylinder is remarkable. Increasing the gap ratio enhances the jet flow passing through the gap, which attaches to the water surface after detaching from the cylinder surface. At this gap width the flow is no longer constrained at the upper surface of the cylinder, and the velocity at the to of the cylinder is higher than that at the bottom. This result, which is confirmed by the mean velocity field, implies that the free surface still influences the cylinder wake at this level of submergence. No reverse flow occurs beneath the free surface and the near-wake does not incline downward. The flow structures at the higher gap ratios of $h^*=0.92$ and 1.13 are very similar to the structure at $h^*=0.709$.

The streamline contours (Figs. 4(a) and (b)) show that in addition to the downward incline of the near-wake of the cylinder observed for systems with $h^*=0.142$ and 0.425, the flow direction of uniform stream beneath the wake region also deflects downward. This phenomenon is barely discernable from the instantaneous velocity
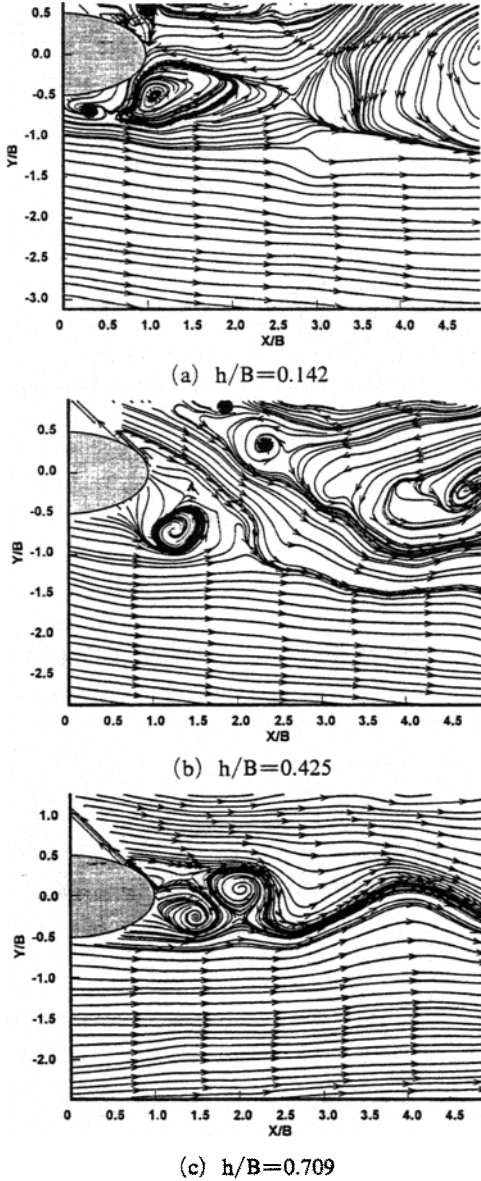
(a) h/B=0.142

(b) h/B=0.425

(c) h/B=0.709

Fig. 4   Streamline contours with respect to the depth of submergence

(a) h/B=0.142

(b) h/B=0.425

(c) h/B=0.709

Fig. 5   Variations of mean velocity profiles

vector fields. At $h^*=0.709$, however, the flow direction of uniform stream remains horizontal. The streamline contours for the gap ratios of $h^*=0.142$ and 0.425 also show the reverse flow beneath the water surface and the range of the swirl in the wake region. For a gap ratio of 0.709, Fig. 4(c) shows the vortex shedding from the cylinder and the disappearance of reverse flow in the near
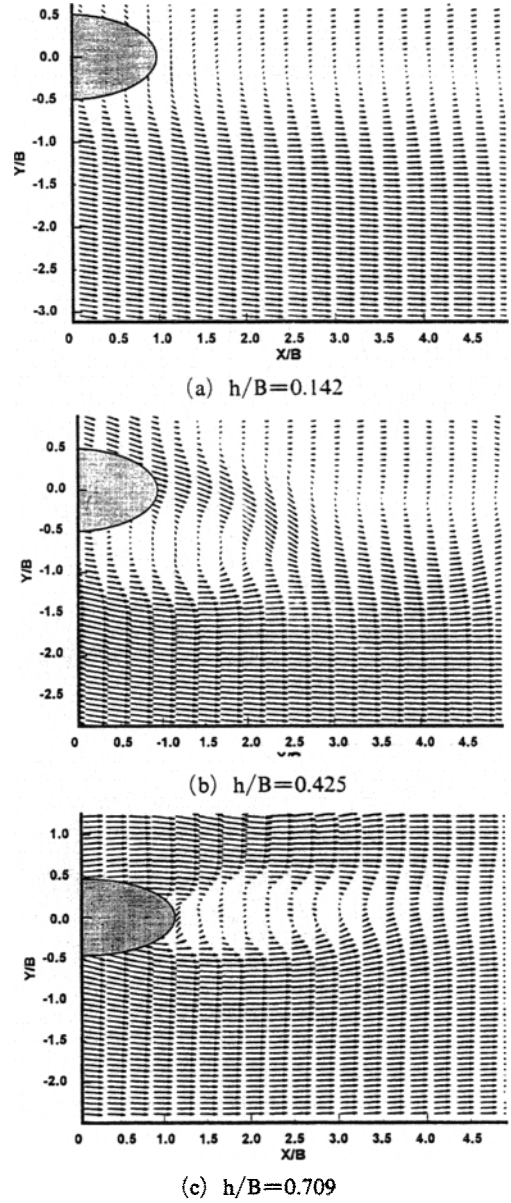
wake. The position of the vortex is clearly observed in all cases.

3.2   Mean flow fields

To study the time-averaged flow structure 350 instantaneous velocity fields were obtained for each experimental condition. These velocity fields were ensemble averaged to obtain spatial
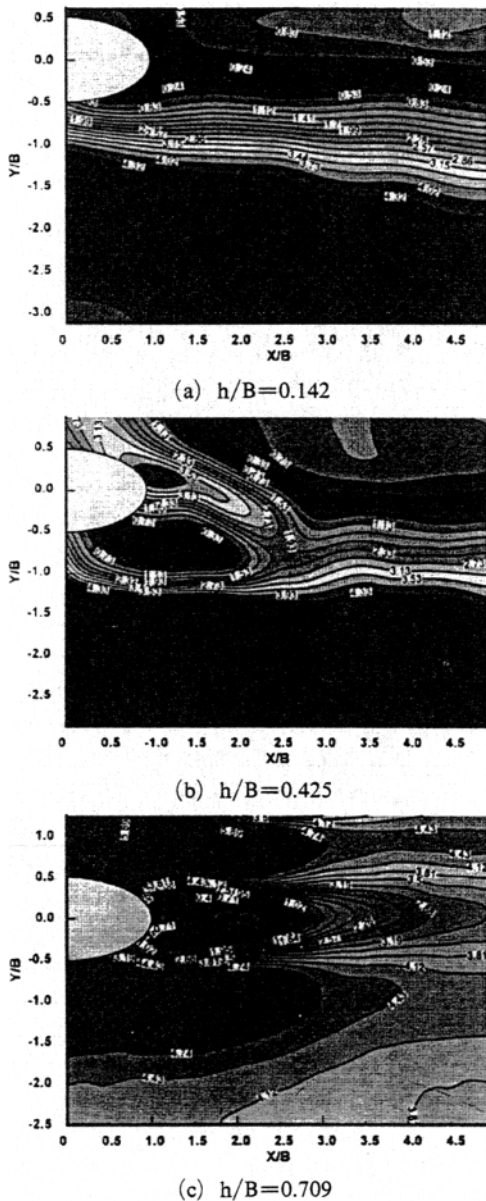
(a) h/B=0.142

(b) h/B=0.425

(c) h/B=0.709

Fig. 6 Contour plots of streamwise mean velocity

distributions of the mean velocity and mean vorticity field. Probing the turbulent structure of the flow interaction was of particular interest in these experiments.

The mean velocity profiles and contour plots of the streamwise mean velocity are illustrated in Figs. 5 and 6 respectively. For $h^*=0.142$ (Fig. 5 (a)), the velocity of Coanda flow formed at the upper surface of the cylinder is higher than the

velocity in the near wake, but is still lower than the velocity in the mixing layer. The width of the near-wake expands as the flow goes downstream. In addition, the wake is inclined slightly downward; the deflection angle with respect to the horizontal is smaller than that for a circular cylinder under similar experimental conditions. At $h^*=0.425$, the flow is still constrained to pass through the gap between the elliptic cylinder and the free surface. The velocity above the elliptic cylinder is therefore lower than that below the cylinder. Compared with the behavior at $h^*=0.142$, the deflection angle of the wake is slightly lower, the velocity of reverse flow in the proximity of the free surface is higher, whereas the region of reverse flow is smaller. When the gap ratio is increased to $h^*=0.709$, the wake region behind the cylinder is nearly horizontal and roughly symmetric with respect to the major axis of the elliptic cylinder. No reverse flow is observed in near-wake; however, the velocity of the upper shear layer is higher than that of the lower shear layer.

Figure 7 shows vorticity contours for the three cylinder submergence depths. At a gap ratio of $h^*=0.142$ (Fig. 7(a)), the entire flow field is dominated by positive vorticity, especially over area of the shear layer developed from the bottom of cylinder. The maximum vorticity is observed near the lower side of the cylinder. The minimum vorticity, however, occurs in a small area close to the upper surface of the cylinder.

At gap ratio of $h^*=0.425$(Fig. 7(b)), the substantial jet flow causes the vorticity of the flow on both sides of the jet to be enhanced. The peak of negative vorticity is located near the bottom edge of the jet; its magnitude is similar to the peak of positive vorticity near the bottom of the elliptic cylinder. On further increase of the gap ratio to $h^*=0.709$ (Fig. 7(c)), the vorticity contours at the top and bottom sides of the cylinder become nearly symmetric with respect to the major axis of the elliptic cylinder. However, the magnitude of the negative vorticity on the upper side is higher than that of the positive vorticity on the lower side. This behaviour may result from the stronger shear flow caused by the influence of the free
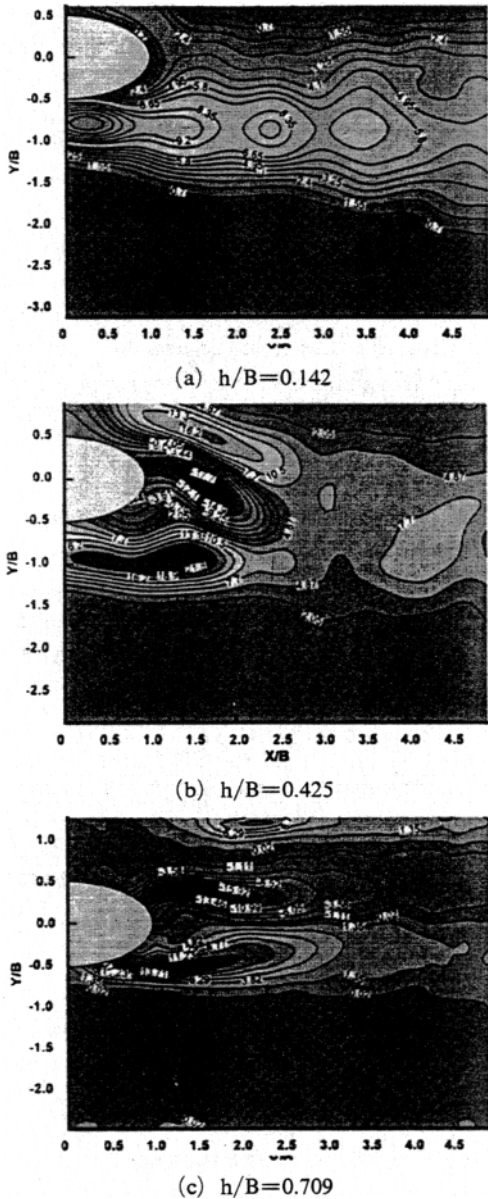
(a) h/B=0.142

(b) h/B=0.425

(c) h/B=0.709

Fig. 7 Contour plots of mean vorticity

surface on the upper surface of the cylinder.

3.3 Turbulent characteristics

Although the instantaneous velocity vector fields show the variation in the flow structure, a detailed investigation of the turbulent structure requires spatial distributions of turbulent statistics such as the turbulent intensity, Reynolds stress and turbulent kinetic energy.

The flow velocity U can be decomposed into its mean value $\langle U \rangle$ and a fluctuating value u'. The Reynolds stress stems from the momentum transferred by the fluctuating velocity, and represents the momentum exchange between the mean velocity field and velocity fluctuations, i. e. the influence of velocity fluctuations on the mean flow field. Here, we are concerned with the influence of the Reynolds stress on the turbulent structure of the flow field.

Figures 8(a), (b), and (c) present the contours of the Reynolds stress for the three typical gap ratios. At a gap ratio of $h^*=0.142$, the Reynolds stress is greater in the mixing layer downstream of the lower side of the cylinder (X/B=1.5) and in the near wake of the cylinder (X/B=3.5). Positive Reynolds stress dominates the entire flow field at this gap ratio. At a gap ratio of $h^*=0.425$ (Fig. 8(b)), the maximum absolute value of the Reynolds stress appears near the location where the jet-like flow detaches from the upper surface of the elliptic cylinder (X/B=1.0). The Reynolds stress at this location has a negative value, and the magnitude of maximum positive Reynolds stress in the near wake is much higher than that case for $h^*=0.142$. This behaviour implies that the existence of the jet flow between the cylinder and water surface greatly intensifies the fluctuating in the near wake. When the gap ratio is increased to $h^*=0.709$ (Fig. 8(c)), the maximum of the positive and negative Reynolds stress are symmetrically distributed near the upper and lower sides of the cylinder. The magnitudes of the positive and negative Reynolds stress are similar, but smaller than the maximum values observed at $h^*=0.142$. The positive and negative values indicate the direction of the Reynolds stress. From the spatial distribution of the Reynolds stress for each case, it can be seen that higher values of the Reynolds stress are commonly observed near locations with stronger shear flow. This indicates that the momentum transfer of the fluctuating velocity is active at these locations.

The Reynolds stress contributes to the redistribution of the kinetic energy of the mean flow field, which leads to a decreased part of the total energy being transferred to the fluctuating
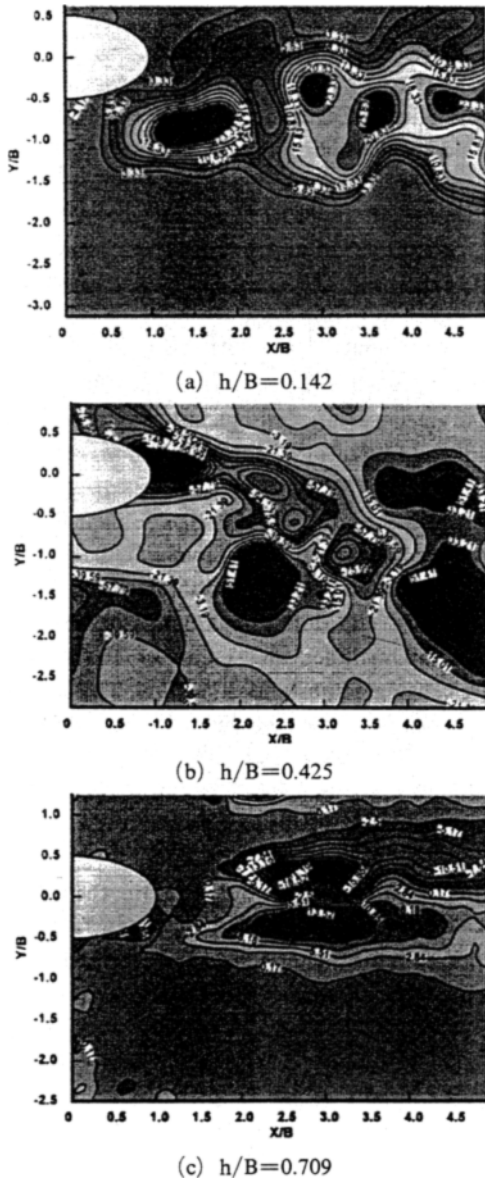
(a) h/B=0.142

(b) h/B=0.425

(c) h/B=0.709

Fig. 8   Contour plots of Reynolds shear stress $u'v'$
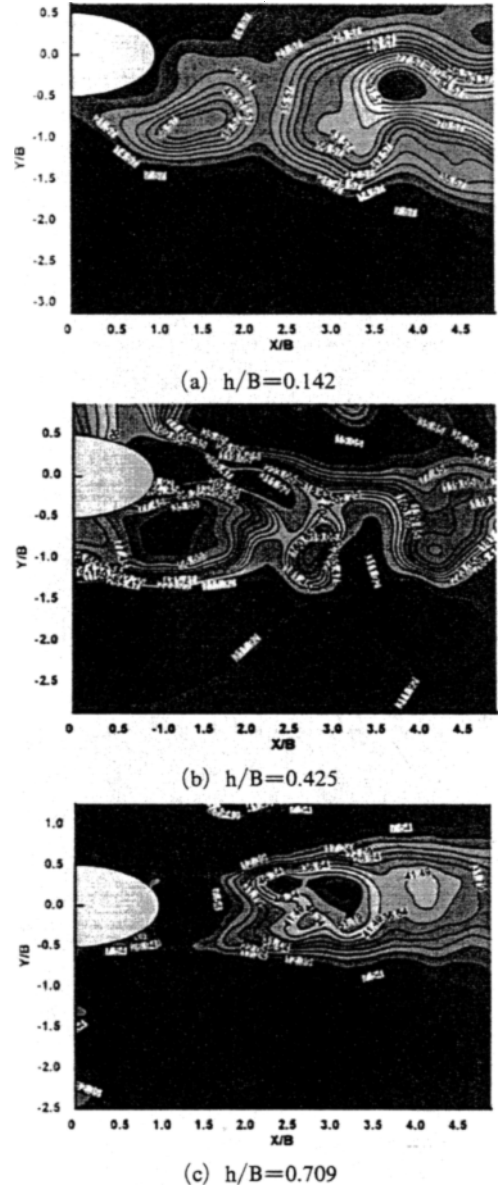

(a) h/B=0.142

(b) h/B=0.425

(c) h/B=0.709

Fig. 9   Contours of turbulence kinetic energy

flow and transformed to turbulent kinetic energy. The contours of the turbulent kinetic energy for each case were compared and the results are shown in Fig. 9. This figure shows that in the near-wake of the cylinder, where the Reynolds stress has higher values, the turbulent kinetic energy also has higher values. This is attributed to the fact that the fluctuating flow obtained more energy with the affect of Reynolds stress, losing

energy of mean flow field is the source of turbulent kinetic energy, the procedure of energy transform is kept by the work of Reynolds stress. The turbulent kinetic energy in the flow field at a gap ratio of $h^*=0.425$ is much higher than that of other two cases. The magnitude of turbulent kinetic energy is low at locations out of the near weak for each case.

The spatial distributions of the streamwise tur-

bulence intensity, shown in Fig. 10, show that the turbulence intensity has a large value at the gap ratio of $h^*=0.425$. The large intensity at this gap ratio results from the high-speed jet flow above the cylinder, which makes the near-wake more active in turbulent mixing. For the larger gap ratio of $h^*=0.709$, the position of the turbulence intensity distribution is nearly symmetric in the near wake region.
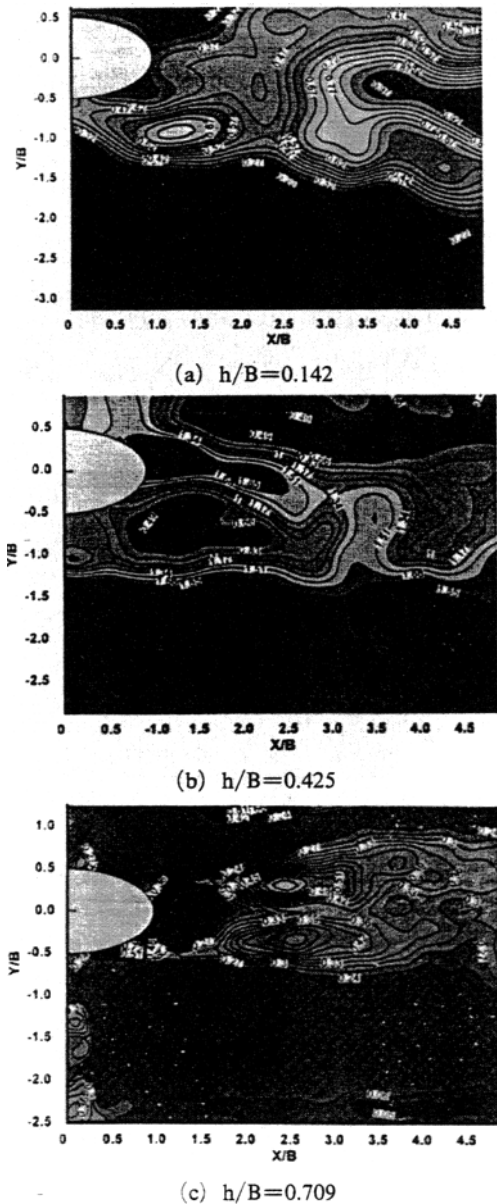

(a) h/B=0.142

(b) h/B=0.425

(c) h/B=0.709

Fig. 10 Contours of streamwise turbulence intensity

4. Conclusion

The effect of a free surface on the near-wake behind an elliptic cylinder was investigated experimentally by varying the gap ratio ($h^*=h/B$) between the cylinder and the water surface. An elliptic cylinder of axis ratio AR=2 was used in these experiments. For comparison, the gap ratio was adjusted to approach the flow condition of a circular cylinder beneath the water surface.

At small gap ratios, the on-coming flow is constrained to pass through the gap between the cylinder and free surface. In the near wake behind the elliptic cylinder a large-scale reverse flow forms beneath the free surface, leading to a downward deflection of the wake. On increasing the gap ratio, the deflection angle decreases slightly. In addition, the Coanda effect forms above the cylinder and enhances the adjacent flow, causing a substantial jet flow. This jet flow brings about active turbulent mixing, increasing the turbulent intensity in the near wake. The deflection angle of the near-wake is smaller than that found in previous experiments using a circular cylinder(Sheridan et al., 1996).

On further increase of the gap ratio, the Coanda wake tends to detach from the upper surface of the elliptic cylinder and attach to the free surface. The flow structure is nearly unchanged above a gap ratio of $h^*=0.709$. Regular vortices are shed from both sides of the cylinder and are nearly symmetric with respect to the major axis of the elliptic cylinder. However, the presence of the free layer causes the upper shear layer of the wake to have a slightly higher velocity than the lower shear layer.

The turbulent statistics show larger values for the gap ratio of $h^*=0.425$ than for the other cases, while the statistics for $h^*=0.142$ and $h^*=0.709$ are at a similar level.

Acknowledgements

References

Angrilli, F. and Bergamashi, S., 1982, "Investigation of Wall Induced Modifications to Vortex Shedding from a Circular Cylinder," *Journal of Fluids Engineering*, Vol. 104, pp. 518~522.

Bearman, P. W. and Zdravkovich, M. M. 1978, "Flow Around a Circular Cylinder near a Plane Boundary," *Journal of Fluid Mechanics*, Vol. 89, pp. 33~47.

Choi, J. H. and Lee, S. J. 2000, "Ground Effect of Flow Around an Elliptic Cylinder in a Turbulent Boundary Layer," *Journal of Fluids and Structures*, Vol. 14, pp. 697~709.

Lin, J. C., et al. 1995, "Instantaneous Structure of the Near-Wake of a Circular Cylinder: on the Effect of Reynolds Number," *Journal of Fluids and Structures*, Vol. 9, pp. 409~418.

Lin, J. C., et al. 1996, "Controlled Motion of a Cylinder Through a Free Surface: Effect of Depth of Penetration," *Journal of Fluid and Structures*, Vol. 10, pp. 309~317.

Oshkai, P. and Rockwell, D. 1999, "Free Surface Wave Interaction with a Horizontal Cylinder," *Journal of Fluid and Structures*, Vol. 13, pp. 935~954.

Sheridan, J., et al. 1997, "Flow Past a Cylinder Close to a Free Surface," *Journal of Fluid Mechanics*, Vol. 33, pp. 1~30.

Shin, D. S., et al. 2000, "Velocity Field Measurements of Flow Inside Snout of Continuous Hot-Dip Galvanizing Process Using a Single-Frame PIV Technique," *ISIJ Int.*, Vol. 40, pp. 484~490.